

Effects of asymmetric coupling and boundary on the dynamic behaviors of a random nearest neighbor coupled system

Ling Xu(徐玲) and Lei Jiang(姜磊)

Citation: Chin. Phys. B, 2024, 33 (**6**): 060503. DOI: 10.1088/1674-1056/ad3b86
Journal homepage: http://cpb.iphy.ac.cn; http://iopscience.iop.org/cpb

What follows is a list of articles you may be interested in

Dynamics and synchronization of neural models with memristive membranes under energy coupling

Jingyue Wan(万婧玥), Fuqiang Wu(吴富强), Jun Ma(马军), and Wenshuai Wang(汪文帅)
Chin. Phys. B, 2024, 33 (**5**): 050504. DOI: 10.1088/1674-1056/ad1dcc

Chimera states of phase oscillator populations with nonlocal higher-order couplings

Yonggang Wu(伍勇刚), Huajian Yu(余华健), Zhigang Zheng(郑志刚), and Can Xu(徐灿)
Chin. Phys. B, 2024, 33 (**4**): 040504. DOI: 10.1088/1674-1056/ad1481

Synchronization-desynchronization transitions in networks of circle maps with sinusoidal coupling

Yun Zhai(翟云), Jinghua Xiao(肖井华), and Zhigang Zheng(郑志刚)
Chin. Phys. B, 2023, 32 (**6**): 060505. DOI: 10.1088/1674-1056/acc062

Quasi-synchronization of fractional-order complex networks with random coupling via quantized control

Hongwei Zhang(张红伟), Ran Cheng(程然), and Dawei Ding(丁大为)
Chin. Phys. B, 2023, 32 (**11**): 110501. DOI: 10.1088/1674-1056/acedf4

Diffusive field coupling-induced synchronization between neural circuits under energy balance

Ya Wang(王亚), Guoping Sun(孙国平), and Guodong Ren(任国栋)
Chin. Phys. B, 2023, 32 (**4**): 040504. DOI: 10.1088/1674-1056/ac7bff

---

Effects of asymmetric coupling and boundary on the dynamic behaviors of a random nearest neighbor coupled system

Ling Xu(徐玲)[1] and Lei Jiang(姜磊)[2,†]

[1] *School of Mathematical Sciences, Sichuan Normal University, Chengdu* 610066, *China*
[2] *School of Mathematics and Statistics, Linyi University, Linyi* 276000, *China*

(Received 2 February 2024; revised manuscript received 25 March 2024; accepted manuscript online 7 April 2024)

This study investigates the dynamical behaviors of nearest neighbor asymmetric coupled systems in a confined space. First, the study derivative analytical stability and synchronization conditions for the asymmetrically coupled system in an unconfined space, which are then validated through numerical simulations. Simulation results show that asymmetric coupling has a significant impact on synchronization conditions. Moreover, it is observed that irrespective of whether the system is confined, an increase in coupling asymmetry leads to a hastened synchronization pace. Additionally, the study examines the effects of boundaries on the system's collective behaviors via numerical experiments. The presence of boundaries ensures the system's stability and synchronization, and reducing these boundaries can expedite the synchronization process and amplify its effects. Finally, the study reveals that the system's output amplitude exhibits stochastic resonance as the confined boundary size increases.

Keywords: asymmetric coupled, confined space, synchronization, stochastic resonance, stability

PACS: 05.40.–a, 05.45.–a, 05.45.Xt, 05.90.+m **DOI:** 10.1088/1674-1056/ad3b86

1. Introduction

It is widely accepted that a system characterized by a multitude of interacting individuals is denominated a complex system. Due to its complex characteristics and rich collective behaviors, it has become a research hotspot[1,2] in multiple interdisciplinary fields and is therefore widely used in biology, engineering, and even social sciences.[3–5] The complexity is not only reflected in the number of individuals contained in the system and the degree of freedom of the system, but also in the form of interaction between individuals, and these forms of interaction are usually modeled as coupling, which can be realized information exchange within complex systems, such as biochemical reactions of positive feedback and negative feedback regulation processes in multicellular biological systems,[6] power distribution, and fault identification networks in power grids.[7] These couplings can be established as regular networks, such as global coupling,[8] nearest neighbor coupling,[9] and star coupling,[10] or they can be established as random networks, small-world networks, etc.[11]

There are various collective behaviors of complex systems, and synchronicity is one of the most basic manifestations and applications.[12] The mechanisms behind the cooperative behavior of complex systems are directly related to synchronization. For example, clock synchronization in power systems ensures the stability of power frequency and accurate power dispatch,[13] and the phenomenon of synchronous flashing in groups of fireflies is another example.[14] Therefore, the synchronization mechanism behind complex systems has received extensive attention from researchers. Existing research has pointed out that the coupling form and the introduction of noise have an important impact on the synchronization of the system.[15] Initially, it was generally believed that noise would destroy the synchronization of the system, whereas coupling usually maintained the synchronization of the system.[16] However, the researchers later discovered that noise can also promote complete synchronization between subsystems. For example, the introduction of noise enhances the synchronization behavior of nonlinear coupling systems.[17] The introduction of dichotomous noise in stochastic bistable systems significantly enhances the phase synchronization effect.[18] The authors in Ref. [19] found that the impact of noise on the contraction domain is greater than the impact on the expansion domain, and explained the internal mechanism of perfect synchronization caused by noise. However, in most cases, especially for non-deterministic complex systems, it is not easy to obtain precise synchronization conditions. In addition, as the scale and complexity of the system increase, how to ensure the stability of the system becomes increasingly important. Stability is the ability of a system to return to an equilibrium state when subjected to external disturbances or internal noise.[20] In stochastically coupled systems, the stability conditions are more stringent because the system is not only disturbed by external perturbations but also by internal noise. Researchers have proposed some methods to analyze the stability of complex systems. These methods include Lyapunov stability, Hamiltonian stability, impulse stability, etc.[21] These stability conditions provide important theoretical tools for analyzing and predicting system behav-

[†]Corresponding author. E-mail: jl12130o0o@163.com

© 2024 Chinese Physical Society and IOP Publishing Ltd

ior. The asymmetry of complex systems has a crucial impact on their collective behaviors.[22] Asymmetry can arise not only through the system's special network topology, but also through asymmetric coupling. In practical applications, asymmetric coupling widely exist in complex systems such as signal transmission,[23] brain neural networks,[24] swarm intelligence networks,[25] and biomolecular motors,[26] and produce rich group effects, such as stochastic resonance (SR), cluster synchronization, etc. For example, Zhang *et al.*[23] studied signal transmission under a one-way coupled bistable system and discovered SR. Hillier *et al.*[27] found that asymmetric coupling causes chaotic oscillator arrays to exhibit a new form of cluster synchronization. Antonio[28] confirmed the existence of stable synchronization states in asymmetrically coupled homogeneous oscillators. Batra *et al.*[29] found that driven by quadratic asymmetric bipartite noise, the system still exhibits SR when the potential field parameter is zero. Based on the important role of asymmetric coupling in the system, it is necessary to study the collective behavior of complex systems under asymmetric coupling.

In addition, traditional research mainly considers macroscopic systems dominated by pure potential energy, that is, the system is in an unrestricted space. However, systems are sometimes restricted, even mesoscopic.[30,31] Research has found that systems in confined spaces may exhibit completely different dynamic properties. Burada[32] considered the free diffusion of Brownian particles in a dumbbell-shaped microcavity and discovered entropic SR. Zhang *et al.*[33] found that the unrestricted linear overdamped system has no SR, which occurs when the system is restricted. Chen *et al.*[34] studied the collective dynamic behavior of an adjacent coupling chain in unconfined and confined spaces, and found that the existence of boundaries can promote the synchronization and stability of the system, and exhibit more complex SR. Therefore, the scale and shape of space have an important impact on the dynamic properties of the system.

This study will investigate the collective behaviors of nearest neighbor asymmetric coupling chains driven by multiplicative dichotomous noise and cosine periodic forces in a one-dimensional (1D) confined space. The precise stability and synchronization conditions of the unconfined system will be solved and the reliability verified. Discuss the effects of asymmetric coupling, confined space, and other system parameters on synchronization region, synchronization speed, and stability conditions, and analyze their mechanisms. In addition, this study will explore the SR of the system.

The arrangement of this study is as follows: Section 2 mainly introduces the nearest neighbor asymmetric coupling chain model in 1D unconfined and confined spaces. In Section 3, the main results of this article are given through numerical simulation and theoretical derivation. Finally, Section 4 summarizes the conclusions.

2. Model

In the study, we consider a stochastic nearest neighbor asymmetric coupled system. Its dynamics can be described by the following linear over-damped Langevin equation:

$$\begin{cases} \dfrac{\mathrm{d}x_1(t)}{\mathrm{d}t} + (\omega + \xi(t))x_1(t) \\ = \varepsilon_1(x_2(t) - x_1(t)) + A_0\cos(\Omega t), \\ \dfrac{\mathrm{d}x_i(t)}{\mathrm{d}t} + (\omega + \xi(t))x_i(t) \\ = \varepsilon_1(x_{i+1}(t) - x_i(t)) + \varepsilon_2(x_{i-1}(t) - x_i(t)) \\ \quad + A_0\cos(\Omega t), 1 < i < N, \\ \dfrac{\mathrm{d}x_N(t)}{\mathrm{d}t} + (\omega + \xi(t))x_N(t) \\ = \varepsilon_2(x_{N-1}(t) - x_N(t)) + A_0\cos(\Omega t), \end{cases} \tag{1}$$

where $x_i(t)$ represents the displacement of the i-th particle at time t. It is only connected to its nearest two neighbors by linear coupling. In particular, the first particle is only coupled to the second particle, and the last particle is only coupled to the penultimate particle. ε_1 and ε_2 are the coupling strengths with the left neighbor and right neighbor, respectively. The coupling coefficients along different directions are not the same (Fig. 1). $\varepsilon_1(x_{i+1}(t) - x_i(t)) + \varepsilon_2(x_{i-1}(t) - x_i(t)$ is the nearest neighbor force for the i-th ($i = 2, \ldots, N-1$) particle. In particular, the nearest neighbor coupling force for the first particle is $\varepsilon_1(x_2(t) - x_1(t))$. $\varepsilon_2(x_{N-1}(t) - x_N(t))$ is the nearest neighbor coupling force of the last particle. The nearest neighbor coupling model is widely used in the study of the dynamic behavior of the Josephson structure arrays,[35,36] the neural networks,[37] and the coupled protein motors.[35]

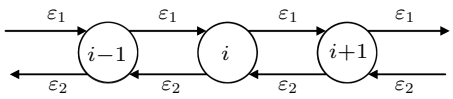


Fig. 1. Coupling diagram of the i-th particle. ε_1 corresponds to the coupling strength with the left neighbor while ε_2 corresponds to the coupling strength with the right neighbor.

$A_0 \geq 0$ and $\Omega > 0$ are the external periodic-driven amplitude and frequency of the system (1), respectively. Fluctuation of the potential field parameter $\omega > 0$ is described by the symmetric dichotomous noise $\xi(t)$.[38–40] It is a random stationary Markovian process that consists of jumps between two values $\pm\sigma$ with $\sigma > 0$. The mean value and the autocorrelation of $\xi(t)$ satisfy

$$\langle \xi(t) \rangle = 0, \quad \langle \xi(t)\xi(s) \rangle = \sigma^2 \mathrm{e}^{-\lambda|t-s|}, \tag{2}$$

where σ is the noise amplitude, λ is the transition rate, and it is the reciprocal of the noise correlation time $\tau_c = 1/\lambda$. Affected by potential field fluctuations, the potential well of particle x_i switches randomly between $V_\pm(x) = (\omega \pm \sigma)x^2/2$.

(i) When $0 < \sigma < \omega$, both potential wells $V_\pm(x)$ open upward. In this case, the particle motion is bounded by the potential field force, driven by external periodic forces and noise to

make a bounded motion near the bottom of the potential field. Thus, both $V_{\pm}(x)$ are in steady states.

(ii) When $0 < \omega < \sigma$, $V_{+}(x)$ opens upwards, but $V_{-}(x)$ opens downwards. Particle x_i may slide to infinity in $V_{-}(x)$ under the action of noise. Thus, $V_{+}(x)$ is stable, but $V_{-}(x)$ is unstable. In this case, the potential field switches randomly between stable and unstable.

Thus, the stability of the output response of the system (1) is not trivial. The physical meaning of this potential energy fluctuation can be found in biological systems, such as the ATP-ADP cyclic potential. In biological systems, ATP releases energy by hydrolyzing the bond, which involves the conversion of energy and ADP. This energy conversion process has similarities with the fluctuations of the model's potential energy. Moreover, the asymmetric coupling in molecular motors will lead the system to be subjected to periodic force driven in the ATP-ADP potential field, which can be seen as an application scenario of the model (1). In Ref. [41], the study of this type of model (1) implies its potential applications in different scenarios. In Ref. [23], the signal transmission of a similar model under one-way coupling conditions was investigated, and it was pointed out that this type of model has widespread applications in open flow systems and one-way driven dynamic chains. In particular, when $N = 1$, system (1) degenerates into a single particle model.[42] It is widely used in many fields, such as problems of fluctuating barrier crossing,[43] enzimatic kinetics,[44] nuclear magnetic resonance,[45] gene expression,[46] and electric circuit.[47] In fact, if one considers the single particle model as a limiting case of a nonlinear problem, dozens of different applications may exist.[42]

Since many real physical systems are always confined, studying confined systems has its practical application interest.[30–34] Thus, in this study, we also consider the asymmetric nearest neighbor coupling chain with N particles in a confined space. Its dynamic model can be described by the following dimensionless linear overdamped Langevin equations:

$$\begin{cases} \dfrac{\mathrm{d}x_1(t)}{\mathrm{d}t} + (\omega + \xi(t))x_1(t) \\ = \varepsilon_1(x_2(t) - x_1(t)) + A_0\cos(\Omega t), \\ \dfrac{\mathrm{d}x_i(t)}{\mathrm{d}t} + (\omega + \xi(t))x_i(t) \\ = \varepsilon_1(x_{i+1}(t) - x_i(t)) + \varepsilon_2(x_{i-1}(t) - x_i(t)) \\ \quad + A_0\cos(\Omega t), \quad 1 < i < N, \\ \dfrac{\mathrm{d}x_N(t)}{\mathrm{d}t} + (\omega + \xi(t))x_N(t) \\ = \varepsilon_2(x_{N-1}(t) - x_N(t)) + A_0\cos(\Omega t), \\ x_n(t) \in [-B, B], \quad n = 1, 2, \ldots, N, \end{cases} \tag{3}$$

where the displacement of the i-th particle $x_i(t)$ is confined to the interval $[-B, B]$ (Fig. 2). When the particle hits the boundary, it is bounced back into $[-B, B]$ with the same speed and opposite direction.

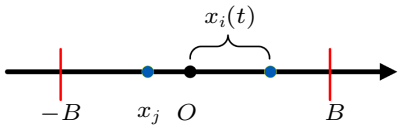


Fig. 2. Schematic diagram of a 1D confined space.

3. Dynamics of asymmetric coupled nearest neighbor systems

3.1. Unconfined model

To analyze the impact of coupling asymmetry on the dynamics nearest neighbor coupling chain. In this section, we give the stability condition and synchronization condition of the system in the unconfined case (system (1)).

3.1.1. Stability condition

The stability discussed here is bounded-input–bounded-output stability of the first and second moments of the particles' displacements. For this purpose, it is necessary to give the complete system of equations satisfied by $\langle x_i \rangle$. Firstly, we average over all realizations of the trajectories of the stochastic Eqs. (1), which gives

$$\begin{cases} \left(\dfrac{\mathrm{d}}{\mathrm{d}t} + \omega + \varepsilon_1\right)\langle x_1\rangle + \langle \xi x_1\rangle - \varepsilon_1\langle x_2\rangle = A_0\cos(\Omega t), \\ \left(\dfrac{\mathrm{d}}{\mathrm{d}t} + \omega + \varepsilon_1 + \varepsilon_2\right)\langle x_i\rangle + \langle \xi x_i\rangle - \varepsilon_1\langle x_{i+1}\rangle - \varepsilon_2\langle x_{i-1}\rangle \\ = A_0\cos(\Omega t), \quad 1 < i < N, \\ \left(\dfrac{\mathrm{d}}{\mathrm{d}t} + \omega + \varepsilon_2\right)\langle x_N\rangle + \langle \xi x_N\rangle - \varepsilon_2\langle x_{N-1}\rangle = A_0\cos(\Omega t). \end{cases} \tag{4}$$

Then, applying the Shapiro–Loginov (SL) formula

$$\langle \xi \cdot \mathrm{d}x_i/\mathrm{d}t\rangle = \mathrm{d}\langle \xi x_i\rangle/\mathrm{d}t + \lambda\langle \xi x_i\rangle,$$

we can get the complete system of equations for $\langle x_i \rangle$. Finally, based on the linear system stability criterion,[48] the stability condition of the first moment $\langle x_i \rangle$ is derived in the following equation:

$$\sigma^2 < \sigma_{\mathrm{sta1}}^2 = \omega^2 + \lambda\omega. \tag{5}$$

Besides, we also need to consider the fluctuation of each particle's displacement, that is, the degree to which each particle deviates from its average displacement, which is described by the variance $\langle \Delta_i \rangle$ of x_i

$$\langle \Delta_i \rangle = \langle (x_i - \langle x_i \rangle)^2 \rangle. \tag{6}$$

Since $\langle \Delta_i \rangle = \langle x_i^2 \rangle - \langle x_i \rangle^2$, it can be seen that when the first moment $\langle x_i \rangle$ is stable, the stability of $\langle \Delta_i \rangle$ is equivalent to the stability of the second moment $\langle x_i^2 \rangle$. Using the SL formula and equation $\mathrm{d}\langle x_i x_j\rangle/\mathrm{d}t = \langle \dot{x}_i x_j\rangle + \langle x_i \dot{x}_j\rangle$, the stability condition of the second moment $\langle x_i^2 \rangle$ for Eq. (1) is as follows:

$$\sigma^2 < \sigma_{\mathrm{sta2}}^2 = \omega^2 + \frac{1}{2}\lambda\omega. \tag{7}$$

The derivation process of inequalities (5) and (7) is given in Appendix A. Because $\sigma^2_{\rm sta2} < \sigma^2_{\rm sta1}$, the stability of the second moment of particles' displacements implies the stability of the first moments. From Eqs. (5) and (7), it can be seen that the stability of the output responds of system (1) only depends on the noise amplitude σ, noise correlation rate λ, and potential field parameter ω, but has nothing to do with the number of particles N, coupling coefficients ε_1, ε_2, and the external periodic force $A_0\cos(\Omega t)$. Therefore, it can be considered that the stability of the system (1) is determined by the random potential field $V_{\pm}(x_i)$.

3.1.2. Synchronization condition

To obtain the synchronization condition of system (1), we need to define new variables $\delta_i = x_{i+1} - x_i, i = 1,\ldots,N-1$. Subtracting the previous one from the latter equation in Eqs. (1) , the following homogeneous linear equations for δ_i are obtained

$$\begin{cases} \left(\dfrac{\mathrm{d}}{\mathrm{d}t} + \omega + \varepsilon_1 + \varepsilon_2\right)\delta_1 + \xi\delta_1 - \varepsilon_1\delta_2 = 0, \\ \left(\dfrac{\mathrm{d}}{\mathrm{d}t} + \omega + \varepsilon_1 + \varepsilon_2\right)\delta_i + \xi\delta_i - \varepsilon_1\delta_{i+1} - \varepsilon_2\delta_{i-1} = 0, \\ 1 < i < N-1, \\ \left(\dfrac{\mathrm{d}}{\mathrm{d}t} + \omega + \varepsilon_1 + \varepsilon_2\right)\delta_{N-1} + \xi\delta_{N-1} - \varepsilon_2\delta_{N-2} = 0. \end{cases} \tag{8}$$

We call the system (1) statistical synchronization if the first moments $\langle\delta_i\rangle, i = 1,\ldots,N-1$ are stable and $\langle\delta_i\rangle = 0$. Similarly, using the SL formula, a complete system of equations including $\langle\delta_i\rangle$ can be obtained. By analyzing the distribution of the eigenvalues of its coefficient matrix, the synchronization condition of system (1) is as follows:

$$\sigma^2 < \sigma^2_{\rm syn} = r^2_{\rm syn} + \lambda r_{\rm syn}, \tag{9}$$

where

$$r_{\rm syn} = \omega + \varepsilon_1 + \varepsilon_2 + 2\sqrt{\varepsilon_1\varepsilon_2}\cos\frac{(N-1)\pi}{N}.$$

We call inequality (9) the synchronization condition, and its proof is given in Appendix B.

Since

$$\begin{aligned} r_{\rm syn} &= \omega + \varepsilon_1 + \varepsilon_2 + 2\sqrt{\varepsilon_1\varepsilon_2}\cos\frac{(N-1)\pi}{N} \\ &\geq \omega + \varepsilon_1 + \varepsilon_2 - 2\sqrt{\varepsilon_1\varepsilon_2} = \omega + (\sqrt{\varepsilon_1} - \sqrt{\varepsilon_2})^2 \geq \omega, \end{aligned}$$

so we have $\sigma^2_{\rm sta1} \leq \sigma^2_{\rm syn}$. Combined with inequalities (5) and (9), it can be seen that when the first moment of the displacement of each particle is stable, the system (1) is statistical synchronization. This is

$$\sigma^2_{\rm sta2} \leq \sigma^2_{\rm sta1} \leq \sigma^2_{\rm syn}. \tag{10}$$

According to the synchronization condition (9), in addition to the potential field parameter ω and noise correlation rate λ, the synchronization interval $(0, \sigma^2_{\rm syn})$ of the system (1) also depends on the number of particles N and the coupling strengths $\varepsilon_1, \varepsilon_2$. This suggests that the system topology affects its synchronization.

3.1.3. Numerical simulation method

In this section, we will verify the main results given in Subsections 3.1.1 and 3.1.2 by numerical algorithm based on the stochastic Euler algorithm.[49] For a sufficiently small time step Δt, the approximate representation of the model (1) in discrete time is

$$\begin{cases} x_1(t_n) = (1 - (\omega + \varepsilon_1)\Delta t - \Delta X(t_{n-1}))x_1(t_{n-1}) \\ \qquad + \varepsilon_1 x_2(t_{n-1}) + A_0\cos(\Omega t_{n-1}), \\ x_i(t_n) = (1 - (\omega + \varepsilon_1 + \varepsilon_2)\Delta t - \Delta X(t_{n-1}))x_i(t_{n-1}) \\ \qquad + \varepsilon_1 x_{i+1}(t_{n-1}) + \varepsilon_2 x_{i-1}(t_{n-1}) \\ \qquad + A_0\cos(\Omega t_{n-1}), 1 < i < N, \\ x_N(t_n) = (1 - (\omega + \varepsilon_2)\Delta t - \Delta X(t_{n-1}))x_N(t_{n-1}) \\ \qquad + \varepsilon_2 x_{N-1}(t_{n-1}) - x_N(t_{n-1})\Delta X(t_{n-1}) \\ \qquad + A_0\cos(\Omega t_{n-1}), \end{cases} \tag{11}$$

where

$$\Delta X(t_{n-1}) = \int_{t_{n-1}}^{t_n} \xi(u)\,\mathrm{d}u. \tag{12}$$

$\Delta t = t_n - t_{n-1}$ is the time step, ΔX_i is the increment of the dichotomous noise $\xi(t)$ during a single time step, which can be simulated through the method proposed in Ref. [50]. Let the number of simulations be K, $x_{i,k}(t)$ denotes the displacement of the i-th particle in the k-th simulation. Thus, when K is large enough, the simulation approximations of the first moment and second moment of the displacement of the i-th particle are

$$\langle x_i(t)\rangle = \frac{1}{K}\sum_{k=1}^{K} x_{i,k}(t), \quad \langle x_i^2(t)\rangle = \frac{1}{K}\sum_{k=1}^{K} x_{i,k}^2(t), \tag{13}$$

respectively. Therefore, the system mean field $\langle S(t)\rangle$ and the mean value of the second moment $\langle S_2(t)\rangle$ can be obtained by the following simulation:

$$\langle S(t)\rangle = \frac{1}{N}\sum_{i=1}^{N}\langle x_i(t)\rangle, \quad \langle S_2(t)\rangle = \frac{1}{N}\sum_{i=1}^{N}\langle x_i^2(t)\rangle. \tag{14}$$

3.1.4. Verification of stability condition

In order to verify the stability conditions of the system (1) (*i.e.* inequalities (5) and (7)), figure 3 gives the curves of the system mean field $\langle S(t)\rangle$ and the second moment $\langle S_2(t)\rangle$ changing with time t under different noise intensities σ^2. Combined with the parameters given in Fig. 3, the stability region threshold of the system's first (second) moment is $\sigma^2_{\rm sta1} = 2$ ($\sigma^2_{\rm sta2} = 1.5$). It can be seen from Fig. 3 that when

the noise intensity σ^2 is less than the noise threshold, the amplitudes of the first (second) moment of the system are always bounded, and the first moment of the system output is a cosine function. However, as the noise intensity σ^2 exceeds the stability condition threshold, the amplitudes of $\langle S(t)\rangle$ and $\langle S_2(t)\rangle$ gradually diverge to unbounded. This is consistent with inequalities (5) and (7).

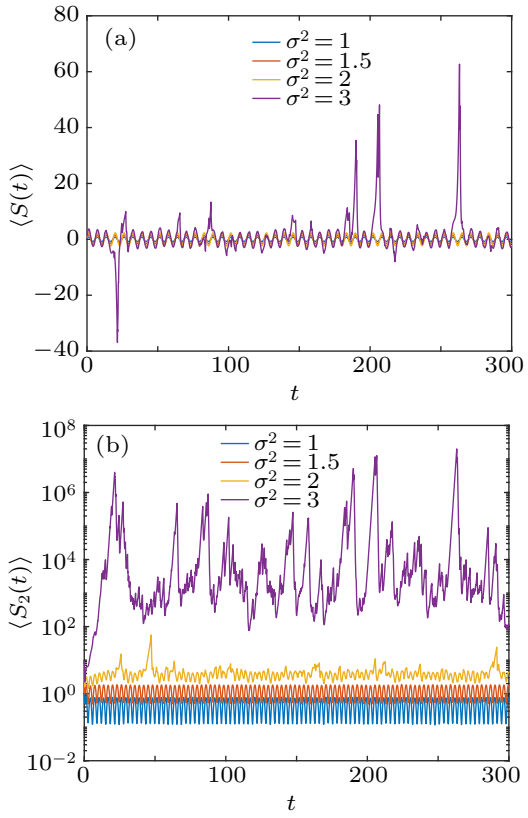


Fig. 3. (a) The curve of the mean field $\langle S(t)\rangle$ as a function of time t with different noise intensities σ^2. (b) The second moment $\langle S_2(t)\rangle$ as a function of time t with different noise intensities σ^2. The other parameters in the two figures are $\Omega=1$, $\omega=1$, $\lambda=1$, $\varepsilon_1=0.1$, $\varepsilon_2=1.9$, $A_0=1$, $K=5000$, $\Delta t=0.01$.

3.1.5. Verification of synchronization condition

In order to verify the synchronization condition given in inequality (9), we first give plots of phase diagram of the synchronization region in σ^2–ε_1–ε_2 coordinate system in Fig. 4(a) and in σ^2–N plane in Fig. 4(b). Figure 4(a) gives a surface plot of the synchronization region as a function of coupling strengths ε_1 and ε_2. The gray surface is the synchronization region boundary ($\sigma^2=\sigma^2_{\rm syn}$), below which is the synchronization region of the system (1). It can be seen that the synchronization region is symmetrical about $\varepsilon_1=\varepsilon_2$. This indicates that reversing the coupling strength of the two directions does not affect the synchronization. In addition, we can also see that the difference in the coupling strength in the two directions has a significant impact on the synchronization region. In order to reflect this change more intuitively, we set $\varepsilon_1+\varepsilon_2=2$, and draw the boundary of the synchronization region under different coupling strength differences as shown in Fig. 4(b). We found that the greater the difference between ε_1 and ε_2, the larger the synchronization region is. And the easier it is for the stochastic asymmetric nearest neighbor coupled system (1) to realize the synchronization. This is because, in system (1), the particles in the middle of the coupling chain is subjected to the coupling force of the two adjacent particles. The two forces are in opposite directions. When the coupling strengths in the two directions are close, the two forces acting on the intermediate particle will partially cancel, and the particles reciprocate in the equilibrium position, making the system more difficult to synchronize. However, with the increase of the difference in the coupling strength between the two directions, the offset portion of the coupling forces in the two directions decreases, making it easier for the system to achieve the synchronization.

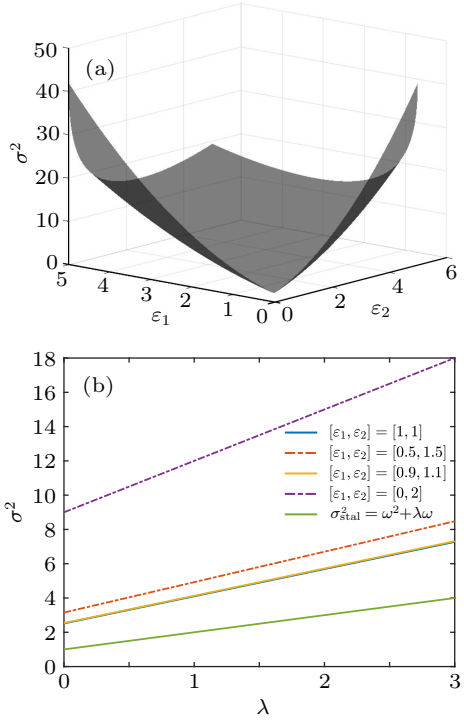


Fig. 4. (a) The synchronization region in σ^2–ε_1–ε_2 coordinate system with $\omega=1$, $\lambda=1$, $N=4$; (b) the synchronization region in σ^2–N plane for different coupling strengths ε_1, ε_2 with $\omega=1$, $N=4$.

Then, we introduce the synchronization error $E_{\rm syn}$ of the first moment of the adjacent particles' displacements as a measurement index:

$$E_{\rm syn}=\frac{1}{N-1}\sum_{i=1}^{N-1}|\langle x_i(t)\rangle-\langle x_{i+1}(t)\rangle|. \tag{15}$$

Figure 5 illustrates the influences of noise intensity σ^2 on synchronization error $E_{\rm syn}$. The synchronization threshold of the system here is $\sigma^2_0=8.0469$. As can be seen from Fig. 5, under each noise intensity, the synchronization error $E_{\rm syn}$ will level off after a period of time. Its stable value increases with the increase of noise intensity σ^2. When $\sigma^2<\sigma^2_0$, the $E_{\rm syn}$ is relatively small (approximately less than 10^{-2}) and the system

is synchronized. When $\sigma^2 > \sigma_0^2$, E_{syn} diverges to 10^5. Thus the system is out of synchronization. The simulation results in Fig. 5 are consistent with the synchronization condition (9).

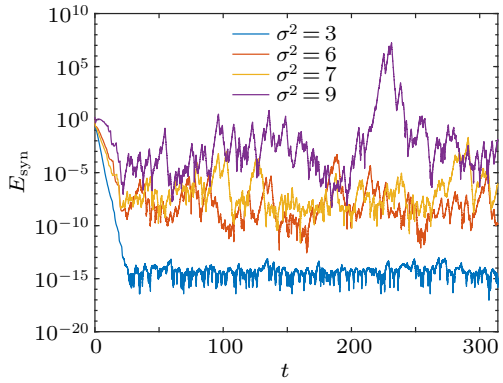


Fig. 5. The curve of synchronization error E_{syn} with time t under different noise intensities σ^2 with $\Omega = 1$, $\omega = 1$, $\lambda = 1$, $\varepsilon_1 = 0.1$, $\varepsilon_2 = 1.9$, $A_0 = 1$, $K = 5000$, $\Delta t = 0.01$.

3.2. Confined model

3.2.1. Numerical simulation method

Since the movement of particles in the confined space is difficult to solve analytically, we use numerical iterative algorithms to analyze their collective dynamic behaviors such as stability, synchronization, and SR. Let $y_i(t_n)$ represent the displacement of the i-th particle at time t_n in the confined space. Firstly, generate a set of random initial values $x_i(t_0)$, let $y_i(t_0) = x_i(t_0)$. Then, equation (16) is used to iterate. When $|x_i(t_n)| \leq B$, set $y_i(t_n) = x_i(t_n)$ and continue to use Eq. (16) to generate $x_i(t_{n+1})$. When $|x_i(t_n)| > B$, we assume that the particle hits the boundary within $[t_{n-1}, t_n]$ and bounces back to the interval, with the speed unchanged and in the opposite direction. Then we obtain $y_i(t_n)$, set $x_i(t_n) = y_i(t_n)$. Use Eq. (16) to iteratively generate $x_i(t_{n+1})$. Therefore, the iterative formula for the displacement of the i-th particle in the confined space is as follows:

$$y_i(t_n) = \begin{cases} \min(-2B - x_i(t_n), B), & x_i(t_n) < -B, \\ x_i(t_n), & |x_i(t_n)| \leq B, \\ \max(2B - x_i(t_n), -B), & x_i(t_n) > B. \end{cases} \tag{16}$$

Figure 6 shows the particle displacement curve in a single simulation in a confined space. As shown in Fig. 6(a), when the boundary value $B = 0.5$, the time–domain plot of the confined system exhibits an approximate square wave. As the boundary gradually increases, as seen in Fig. 6(b) for the boundary value $B = 10$, the time–domain plot of the confined system (3) becomes almost identical to that of the corresponding unconfined system. This means that, in this dataset, the boundary weakens its restriction on the system. Therefore, we can observe that the boundary may have a significant impact on the dynamic properties of the system, and it also suggests that we might be able to optimize the dynamic properties of the system by adjusting the boundary value.

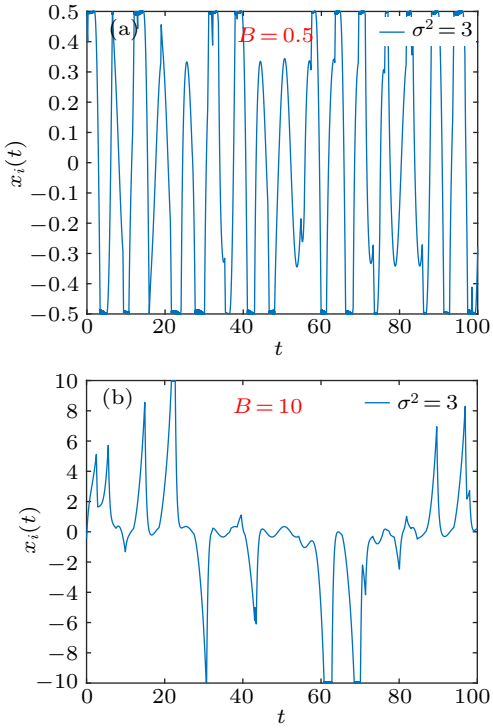


Fig. 6. Single particle displacement in confined space with $\omega = 1, \Omega = 1$, $\lambda = 1$, $A_0 = 1$, $\varepsilon_1 = 0.1$, $\varepsilon_2 = 1.9$, $K = 5000$, $\Delta t = 0.01$, $T = 100$: (a) $\sigma^2 = 0.1$, $B = 0.5$; (b) $\sigma^2 = 3$, $B = 10$.

3.2.2. Stability

In order to analyze the impact of the boundary on the stability of the system, we use Eq. (16) to perform numerical simulation on model (3). Figure 7 show the curves of the first-moment $\langle S(t) \rangle$ and the second-moment $\langle S_2(t) \rangle$ changing with time t at different boundaries B and different noise intensities σ^2. Here, we use different line styles and markers to distinguish each curve. In particular, we have made a partial enlargement in Fig. 7 so that readers can better distinguish curves in different categories. Under the parameters given in the figure, the stability region boundary of the first (second) moment of the unconfined model is $\sigma^2_{\text{sta1}} = 2$ ($\sigma^2_{\text{sta2}} = 1.5$). The average output amplitudes when $\sigma^2 = 1$ and $\sigma^2 = 2$ are 0.7670 and 0.7071, respectively.

From the four subfigures in Fig. 7, we can see that no matter what values B and σ^2 take, the first-moment $\langle S(t) \rangle$ and the second-moment $\langle S_2(t) \rangle$ of the system are stable. In Figs. 7(a) and 7(b), the boundary width is smaller than the original output amplitude when the system is unconfined. The first-order moment amplitude decreases as the noise increases. This is because regardless of the noise increases, the particle displacement can reach the boundary position. The increase in noise will increase the disorder of the particle's single displacement. Therefore, the peaks and troughs of the two particle trajectories do not overlap, so that the average displacement decreases as the noise intensity increases. In Figs. 7(c) and 7(d), the boundary width is greater than the original output amplitude

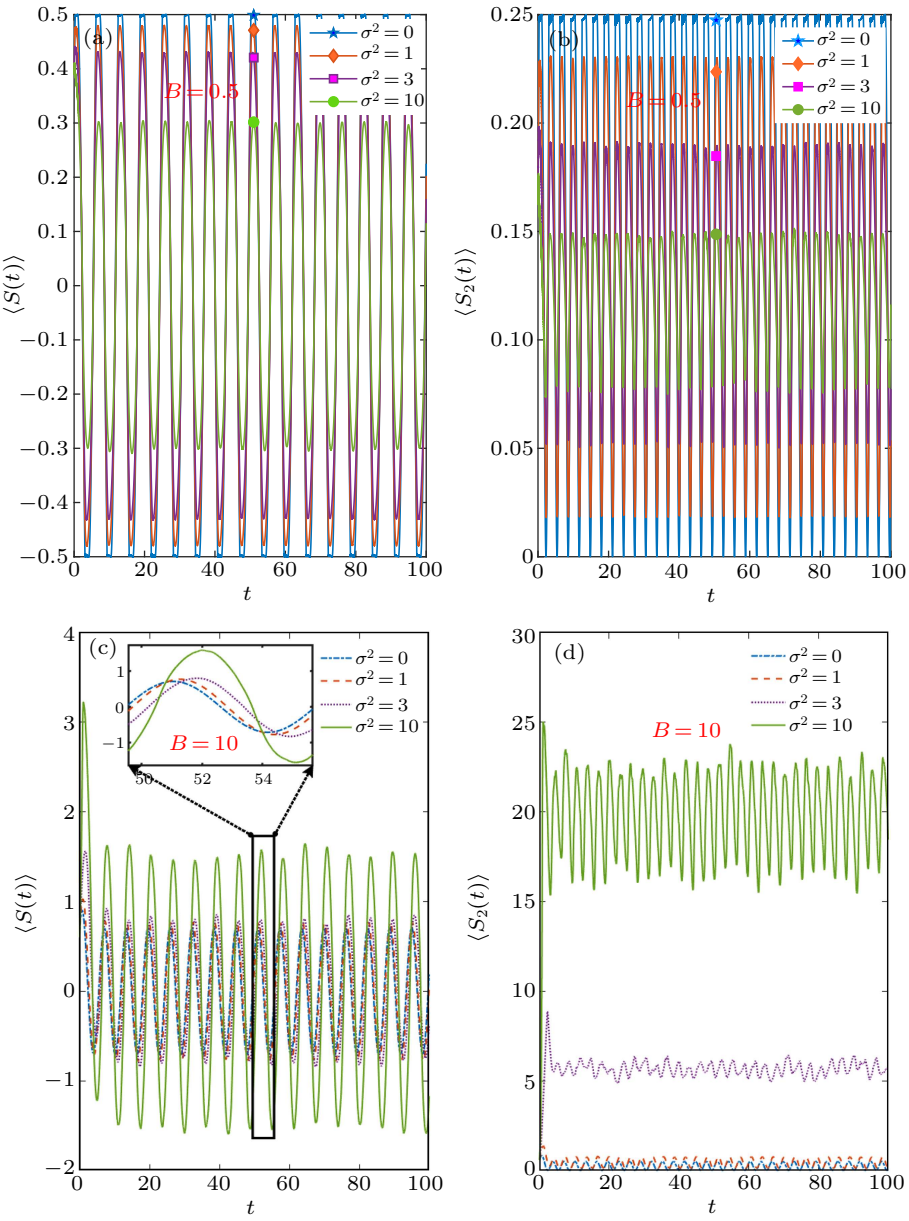


Fig. 7. The system outputs of the first-moment $\langle S(t)\rangle$ and the second-moment $\langle S_2(t)\rangle$ in confined space with $\omega=1$, $\Omega=1$, $\lambda=1$, $A_0=1$, $\varepsilon_1=0.1$, $\varepsilon_2=1.9$, $K=5000$, $\Delta t=0.01$, $T=100$: (a) first-moment $\langle S(t)\rangle$, $B=0.5$; (b) second-moment $\langle S_2(t)\rangle$, $B=0.5$; (c) first-moment $\langle S(t)\rangle$, $B=10$; (d) second-moment $\langle S_2(t)\rangle$, $B=10$.

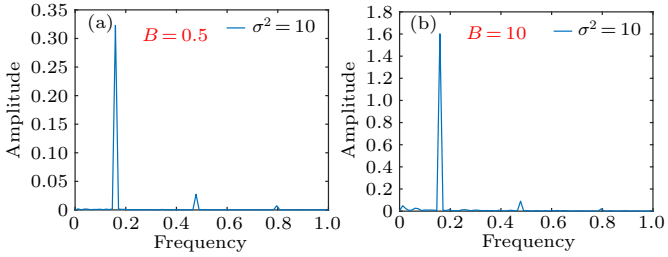


Fig. 8. (a) Frequency–domain diagram of curve $\sigma^2=10$ in Fig. 7(a); (b) frequency–domain diagram of curve $\sigma^2=10$ in Fig. 7(c).

when the system is unconfined. The first-order moment amplitude increases as the noise increases. This is because when the noise intensity is small, the system is stable and the particle displacement does not diverge to the boundary. As the noise intensity increases, the particle motion becomes more disordered and the particle displacement diverges to the boundary more frequently. Therefore, the amplitude of $\langle S(t)\rangle$ increases with the increase of noise. Comparing the uncondined model (1), it can be seen that the boundary plays a decisive role in the stability of system (3). In fact, by performing Fourier transform on the two curves $\sigma^2=10$ in Figs. 7(a) and 7(c) (see Fig. 8), it can be seen that its spectrum is mainly composed of fundamental harmonic with frequency Ω and high-order harmonics with frequency $(2k+1)\Omega$, $k=1,2,\ldots$, as shown in Fig. 8.[33] This also confirms that no matter what values B and σ^2 take, the confined system is always stable.

3.2.3. Synchronization

In this section, we analyze the synchronicity of the confined coupled system (3). Figure 9 depicts the curves of the

average displacement difference $E_{\rm syn}$ of the system as a function of time t under different noise intensities σ^2 and different boundaries B. From this we can see that the system (3) is always synchronized regardless of the noise intensity and boundary values. In Fig. 9(a), it can be seen that as the noise intensity increases, the synchronization speed slows down and the synchronization error gradually increases. Figure 9(b) shows that the larger the boundary of the confined system, the weaker the synchronization control effect, and the slower the synchronization speed. This is primarily due to the fact that noise disrupts the system's orderly output, and the presence of a boundary constraints the movement of particles, leading to a more organized state. Consequently, an increase in noise intensity and boundary width contributes to greater disorder in the system's output, which in turn makes particle synchronization more challenging. This results in a longer time required for synchronization and larger synchronization errors.

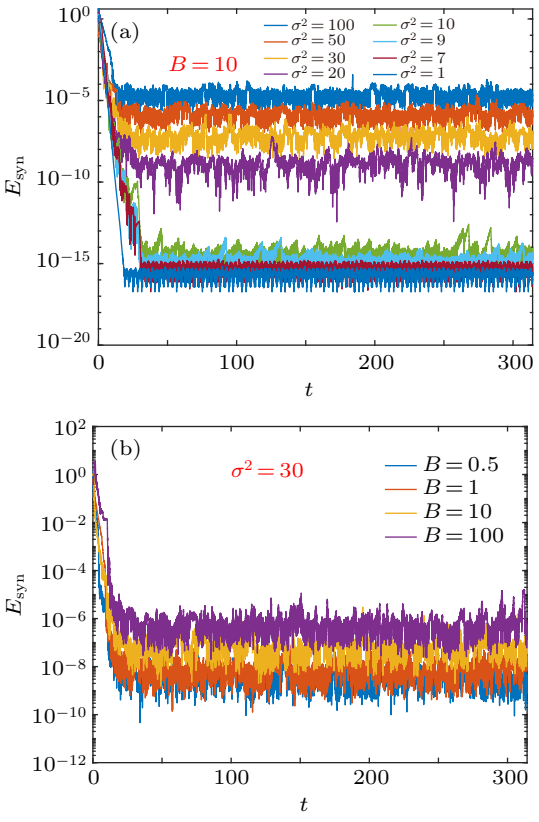


Fig. 9. The curve of the average displacement difference $E_{\rm syn}$ of the system as a function of time t with $\Omega=1$, $\omega=1$, $\lambda=1$, $N=4$, $A_0=1$, $\varepsilon_1=0.1$, $\varepsilon_2=1.9$, $K=5000$, $\Delta t=0.01$, $T=314$: (a) $B=10$, (b) $\sigma^2=30$.

Figure 10 depicts the curves of $E_{\rm syn}$ at different coupling strengths in confined and unconfined spaces. Comparing Figs. 10(a) and 10(b), it can be seen that whether in the confined space or an unconfined space, the increase in coupling asymmetry will speed up the synchronization speed of the system, making the system enter the synchronization state faster. This is because an increase in the coupling asymmetry in the two directions will make the forces on the intermediate particles in the coupling chain more unbalanced in the two directions, reducing the loss of the coupling force within the system, making it easier for the movements of each particle to become consistent, thereby speeding up system synchronization. It can be seen from Figs. 10(b) and 10(c) that the confined system (3) is always synchronized regardless of the coupling strengths. Furthermore, figure 10(c) shows that increasing coupling strength or coupling asymmetry not only speeds up synchronization but also reduces synchronization errors. This is mainly due to the fact that the increase in coupling strength or coupling asymmetry suppresses the randomness of the noise, making the system output more orderly.

Figure 11 depicts the curves of $E_{\rm syn}$ at different particle number N in confined and unconfined spaces. It can be seen from the two sub-figures in Fig. 11 that the increase in the number of particles will slow down the synchronization speed of the system, whether in a confinted space or an unconfined space. In addition, figure 11(b) indicates that the convergence value of $E_{\rm syn}$ will increase with the number of particles. This is mainly because, in the nearest neighbor coupled system, the effect of the coupling force is transmitted one by one through adjacent particles. Increasing the number of particles will increase the propagation distance of the coupling force. Therefore, the more particles there are, the longer the synchronization time will be, and the greater the synchronization error will be.

From Figs. 9–11, we can conclude that, unlike the unconfined system (1), the average displacement of particles in the confined system (3) is always synchronous, regardless of the noise intensity σ^2, the coupling strengthes ε_1 and ε_2, and the number of particles N. In other words, boundary B plays a decisive role in the synchronization of the system. In addition, the interaction of the four elements B, N, σ^2, and $\varepsilon_1, \varepsilon_2$ will also affect the synchronization speed and synchronization effect of the system. In order to more intuitively analyze the impact of each system parameter on synchronization speed, we introduce the synchronization time $t_{\rm syn}$. Set the threshold $\Delta^*=10^{-8}$, when $E_{\rm syn}<\Delta^*$, we assume that the average displacement of each particle is synchronized, and define the time $t_{\rm syn}$ as

$$t_{\rm syn}=\max\{t|\Delta(t)\geq\Delta^*\}. \tag{17}$$

Figure 12(a) shows the curve of $t_{\rm syn}$ as a function of the coupling difference $\Delta\varepsilon$, where $\Delta\varepsilon=\varepsilon_1-\varepsilon_2$. It can be seen from the figure that the increase in coupling difference in the two directions can shorten the synchronization time. In addition, we also found that as $\varepsilon_1+\varepsilon_2$ increases, the curves decrease more and more slowly. This indicates that increasing the coupling strength in both directions at the same time can also speed up the synchronization speed of the system.

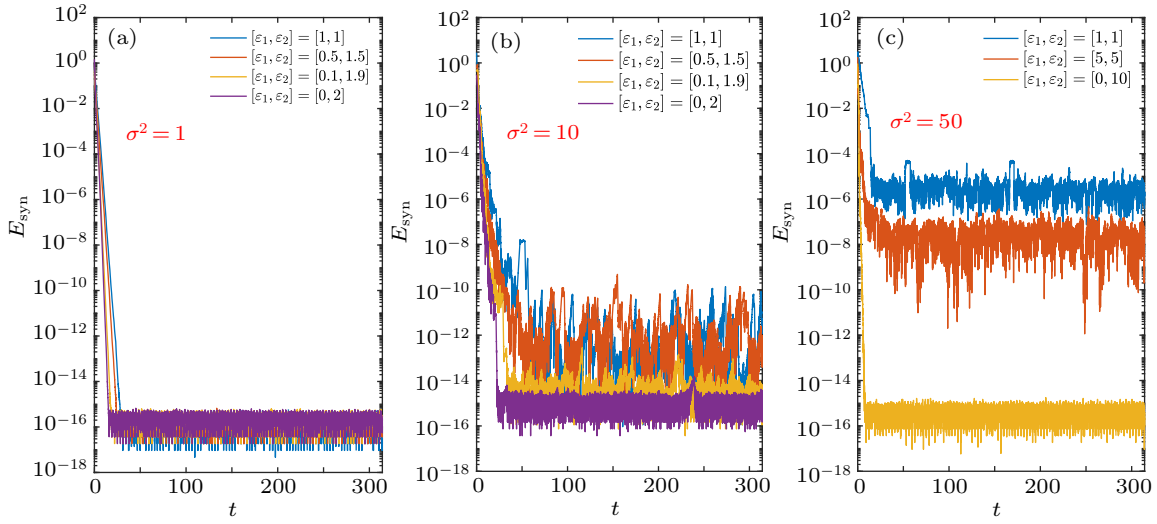


Fig. 10. The curve of the average displacement difference $E_{\rm syn}$ of the system as a function of time t in confined and unconfined spaces with $\Omega=1$, $\omega=1$, $\lambda=1$, $N=4$, $A_0=1$, $B=10$, $K=5000$, $\Delta t=0.01$, $T=314$: (a) unconfined space, $\sigma^2=1$; (b) confined space, $\sigma^2=10$; (c) confined space, $\sigma^2=50$.

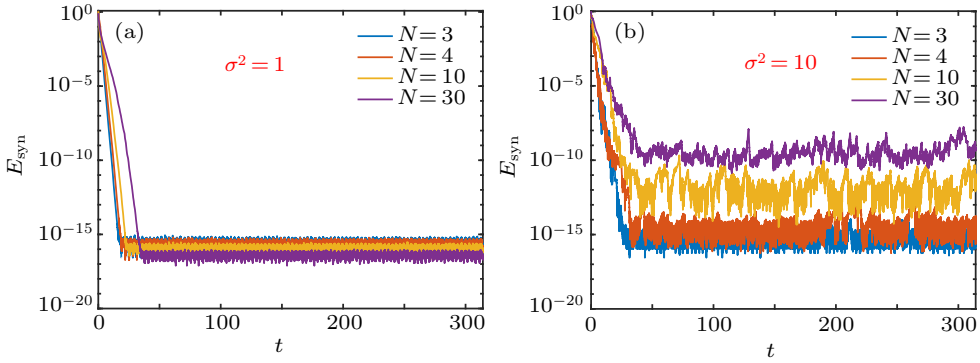


Fig. 11. The curve of the average displacement difference $E_{\rm syn}$ of the system as a function of time t in confined and unconfined spaces with $\Omega=1$, $\omega=1$, $\lambda=1$, $N=4$, $A_0=1$, $B=10$, $\varepsilon_1=0.1$, $\varepsilon_2=1.9$, $K=5000$, $\Delta t=0.01$, $T=314$: (a) unconfined space, $\sigma^2=1$; (b) confined space, $\sigma^2=10$.

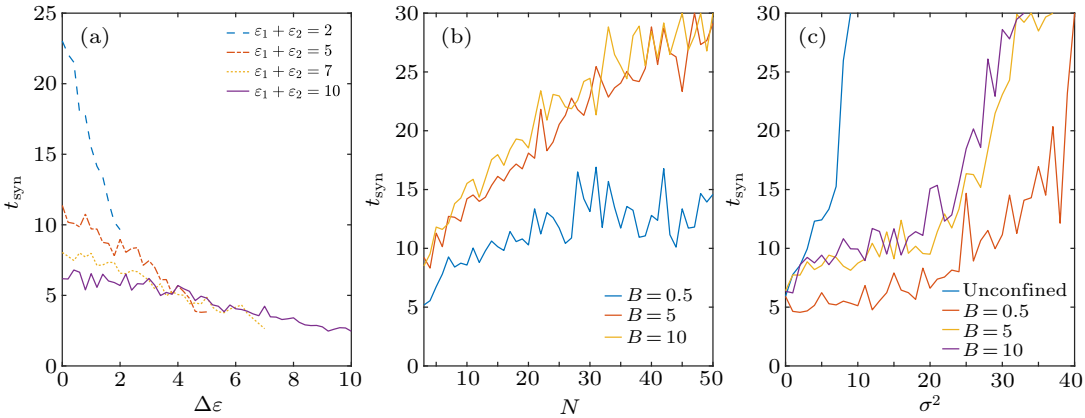


Fig. 12. The curve of synchronization time $t_{\rm syn}$ with $\Omega=1$, $\omega=1$, $\lambda=1$, $A_0=1$, $K=5000$: (a) $\sigma^2=10$, $N=4$, $B=10$; (b) $\varepsilon_1=0$, $\varepsilon_2=2$, $\sigma^2=10$; (c) $N=4$, $\varepsilon_1=0$, $\varepsilon_2=2$.

Figure 12(b) depicts the curve of $t_{\rm syn}$ as a function of the particle number N under different boundary B. It can be seen that the synchronization time increases as the number of particles increases. That is, an increase in the number of particles will hinder the realization of system synchronization. This confirms the conclusion of Fig. 11. Therefore, the more particles there are, the longer the synchronization time will be. In addition, comparing the three curves in Fig. 12(b), we can see that increasing the boundary will increase the synchronization time. The generation mechanism is similar to Fig. 9(b). That is, noise disrupts the average displacement of particles. When B increases, the boundary's restriction on particle movement weakens, making the system output more disordered and the synchronization time increases.

Figure 12(c) depicts the curve of $t_{\rm syn}$ as a function of the noise intensity σ^2 under different boundary B. It can be seen that the synchronization time increases with the increase of noise intensity regardless the boundary. This is mainly because the increase in noise intensity intensifies the disorder of the average particle displacement, thereby inhibiting the synchronization of the confined system.

3.2.4. Stochastic resonance

From the previous analysis, it can be seen that the confined system (3) is always stable and synchronous. The system output is the superposition of several sinusoidal functions. In this section, we use the system output amplitude gain $G = A/A_0$ as the indicator to analyze the SR phenomenon of the system (3), where A is the system output amplitude. For unconfined system (1), due to the synchronicity of the system, the study of SR can be attributed to the study of single particle behavior. The corresponding SR phenomenon, SR condition and mechanism analysis can be found in Ref. [8].

Figure 13 illustrates the influences of the boundary B on the output amplitude gain G. We can see that the parameter stochastic resonance (PSR)[51] to B occurs under different values of σ^2. Its physical mechanisms is as follows: The generation of PSR requires the transfer of part of the noise energy to the system output signal. That is, PSR is the result of the competition between disorder and order in the system. For a given noise intensity, when the boundary is too small, the system output is orderly under the boundary limit. As the boundary increases, the boundary's restriction on particle motion gradually weakens, and the system output becomes disordered. When the boundary is too large, the system output is too disordered. Therefore, a boundary that is too small or too large cannot achieve an optimal match between the noise and the output signal. PSR can only occur in intermediate states. Additionally, in Fig. 13, when $\sigma^2 = 4.5$, as the boundary increases, the system (3) exhibits PSR, and under suitable boundaries, the output amplitude gain G at the peak of the PSR is $G > 1$. This means that with an appropriate boundary, the system's output amplitude can exceed the amplitude of the periodic driving force, leading to amplitude amplification. This phenomenon may occur in nonlinear complex systems, and both the mode of coupling and the topology of complex networks can lead to amplitude amplification, as referenced in Refs. [52,53]. As depicted in Fig. 13 with $\sigma^2 = 4.5$, the combined effect of asymmetric coupling and boundaries in this study causes the linearly coupled system to exhibit nonlinear effects, thereby amplifying the system's output amplitude. Of course, this amplitude amplification can be beneficial, such as efficient conversion of input energy and signal amplification, but it can also be detrimental, as excessively large amplitudes may lead to energy dissipation. When σ^2 increases, the resonance intensity increases, and the position of the resonance peak shifts to the right. This is because an increase in noise intensity σ^2 transfers more noise energy to the signal energy of the system. But B limits the movement range of the particles, thereby limiting the output amplitude of the system. At this time, increasing B can increase G, thereby shifting the resonance peak to the right. Under the parameters given in Fig. 13, the unconfined system (1) is unstable, so there is no SR. This shows that the existence of the boundary weakens the impact of noise on the orderliness of the system and expands the resonance area of the system.

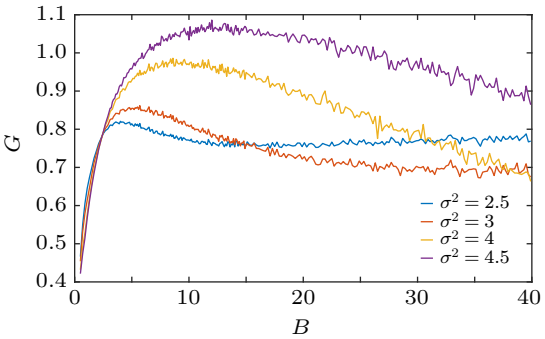


Fig. 13. The curve of the output amplitude gain G with boundary B under different noise intensities σ^2 with $\Omega = 1$, $\omega = 1$, $\lambda = 1$, $A_0 = 1$, $K = 5000$, $N = 4$, $\varepsilon_1 = 0.1$, $\varepsilon_2 = 1.9$.

4. Conclusion

To summarize, we mainly explored the effects of coupling asymmetry and boundary on the dynamic behaviors of an nearest neighbor coupled system with random dichotomous fluctuation potential under an external periodic sine force. Firstly, the precise conditions of stability, synchronization of the asymmetric nearest neighbor coupled unconfined system (1) are derived analytically and verified by numerical simulation. Subsequently, we incorporate the system boundary and explore the impact of the boundary on the system's dynamic behaviors, analyzing its effects on stability, synchronization, and SR.

Asymmetric coupling has an important impact on system synchronization. It is observed that increased coupling asymmetry leads to wider synchronization regions and accelerated synchronization speeds regardless of whether the system is constrained or not. This is mainly caused by the topology of the system. In a nearest neighbor coupling system, a particle is subject to the coupling force of two adjacent particles in the coupling chain, and the two coupling forces are in opposite directions. When the coupling strengths in the two directions are close, the two forces acting on the intermediate particle will partially cancel out, and the particle will reciprocate in the equilibrium position, making the system more difficult to synchronize. However, as the difference in coupling strength in the two directions increases, the resultant force acting on the intermediate particles tends to be in a unified direction, which makes the particles more inclined to move in the same direction, making it easier for the system to achieve synchronization.

Boundary plays the most important role in the collective behaviors of the asymmetric coupled system. Unlike the unconfined system, the existence of boundary makes the system always stable and synchronized. Reducing the boundary can shorten the synchronization time and enable the system to achieve better synchronization effects with the fixed parameters σ^2, N, ε_1, ε_2. In addition, we also observed the PSR of the confined system with respect to the boundary. Compared with the unconfined system, this shows that the boundary can enrich the resonance form of the system and expand the resonance region of the system. Particularly, appropriate boundary values may cause the system's output amplitude can exceed the amplitude of the periodic driving force, leading to amplitude amplification. That is, the combined effect of asymmetric coupling and boundaries in this study causes the linearly coupled system to exhibit nonlinear effects, thereby amplifying the system's output amplitude.

Although the results in this study are carried out around a specific coupling model, its method can be extended to other regular coupling networks such as star coupling networks. Besides, we believe that these conclusions in this study are highly generalizable given that asymmetric coupled confined systems are widely present in various biological and physical mesoscopic systems. Through these studies, we can better understand the dynamical behavior of the system and design more stable and efficient systems for practical problems, and expected to be very useful for further investigation of synchronous control and SR of other complex coupled systems.

Appendix A: Appendix for Subsection 3.1.1

In this section, the corresponding stability conditions both for the first and second moments of the particles' displacements are derived. To analyze the stability of the first moment of the system (1), we first give the complete system of equations satisfied by $\langle x_i\rangle$. Averaging over all realizations of the trajectories of the stochastic Eqs. (1), we get Eqs. (4). A new coupling term $\langle \xi x_i\rangle$ appears in Eqs. (4), in order to solve it, we multiply each equation in system (1) by ξ and take the average. Applying the Shapiro–Loginov formula $\langle \xi \cdot \mathrm{d}x_i/\mathrm{d}t\rangle = \mathrm{d}\langle \xi x_i\rangle/\mathrm{d}t + \lambda\langle \xi x_i\rangle$, we have

$$\begin{cases} \left(\dfrac{\mathrm{d}}{\mathrm{d}t}+\lambda+\omega+\varepsilon_1\right)\langle \xi x_1\rangle + \sigma^2\langle x_1\rangle - \varepsilon_1\langle \xi x_2\rangle = 0, \\ \left(\dfrac{\mathrm{d}}{\mathrm{d}t}+\lambda+\omega+\varepsilon_1+\varepsilon_2\right)\langle \xi x_i\rangle + \sigma^2\langle x_i\rangle \\ -\varepsilon_1\langle \xi x_{i+1}\rangle - \varepsilon_2\langle \xi x_{i-1}\rangle = 0, \quad 1<i<N, \\ \left(\dfrac{\mathrm{d}}{\mathrm{d}t}+\lambda+\omega+\varepsilon_2\right)\langle \xi x_N\rangle + \sigma^2\langle x_N\rangle - \varepsilon_2\langle \xi x_{N-1}\rangle = 0. \end{cases} \tag{A1}$$

Equations (4) and (A1) can be written in the following matrix form:

$$\frac{\mathrm{d}\boldsymbol{X}}{\mathrm{d}t} + \tilde{\boldsymbol{U}}\boldsymbol{X} = \boldsymbol{F}(t), \tag{A2}$$

where $\boldsymbol{X} = (\langle x_1\rangle,\ldots,\langle x_n\rangle,\langle \xi x_1\rangle,\ldots,\langle \xi x_N\rangle)$, $\boldsymbol{F}(t) = (A_0\cos(\Omega t),\ldots,A_0\cos(\Omega t),0,\ldots,0)$,

$$\tilde{\boldsymbol{U}} = \begin{pmatrix} U & E \\ \sigma^2 E & \lambda E + U \end{pmatrix},$$

$$U = \begin{pmatrix} \omega+\varepsilon_1 & -\varepsilon_1 & & & \\ -\varepsilon_2 & \omega+\varepsilon_1+\varepsilon_2 & -\varepsilon_1 & & \\ & & \ddots & & \\ & & -\varepsilon_2 & \omega+\varepsilon_1+\varepsilon_2 & -\varepsilon_1 \\ & & & -\varepsilon_2 & \omega+\varepsilon_2 \end{pmatrix},$$

where E is the identity matrix. The first moment of particles' displacement of the system (1) is stable if and only if the roots of the characteristic equation $r(s) = |sE+\tilde{\boldsymbol{U}}|$ of Eq. (A2) are all distributed in the left-half complex plane, that is, the eigenvalues of matrix $\tilde{\boldsymbol{U}}$ are all distributed in the right-half complex plane.

Theorem A1 The first moment of particles displacements of the asymmetric nearest neighbor coupled system (1) is stable if and only if $\sigma^2 < \sigma^2_{\mathrm{sta1}} = \omega^2 + \lambda\omega$.

Proof Let $f(k) = |kE - \tilde{\boldsymbol{U}}|$, the roots of $f(k)$ are the eigenvalues of the matrix $\tilde{\boldsymbol{U}}$. Simplifying $f(k)$, we have

$$\begin{aligned} f(k) &= |kE - \tilde{\boldsymbol{U}}| \\ &= \begin{vmatrix} kE-U & -E \\ -\sigma^2 E & (k-\lambda)E-U \end{vmatrix} \\ &= |(kE-U)[(k-\lambda)E-U] - \sigma^2 E|. \end{aligned} \tag{A3}$$

Let the eigenvalues of N order square matrix U be $r_1,\ldots,r_N$, set $r_{\mathrm{sta1}} = \min\limits_{1\le i\le N}\{r_i\}$. The Jordan standard form of U is $J = P^{-1}UP$. Thus,

$$\begin{aligned} f(k) &= |P^{-1}||(kE-U)[(k-\lambda)E-U] - \sigma^2 E||P| \\ &= |P^{-1}(kE-U)PP^{-1}[(k-\lambda)E-U]P - P^{-1}\sigma^2 EP| \\ &= |(kE-P^{-1}UP)[(k-\lambda)E-P^{-1}UP] - \sigma^2 P^{-1}EP| \\ &= |(kE-J)[(k-\lambda)E-J] - \sigma^2 E| \\ &= \prod_{i=1}^{N}[(k-r_i)(k-\lambda-r_i) - \sigma^2]. \end{aligned} \tag{A4}$$

According to Eq. (A4), the N roots of $f(k)=0$ are $k_i = r_i + (\lambda \pm \sqrt{\lambda^2+4\sigma^2})/2$, $i = 1,\ldots,N$. The first moment of particles displacements of the system (1) is stable if and only if the smallest root of $f(k)$ is greater than 0. This is, $r_{\mathrm{sta1}} + (\lambda - \sqrt{\lambda^2+4\sigma^2})/2 > 0$. By direct calculations, we have $\sigma^2 < r^2_{\mathrm{sta1}} + \lambda r_{\mathrm{sta1}}$. Since the sum of each row of U is ω, ω is one of the eigenvalues of U. From Gerschgorin circle theorem,[54] we have $r_{\mathrm{sta1}} = \omega$. In summary, the first moment of particles' displacements of the system (1) is stable if and only if $\sigma^2 < \omega^2 + \lambda\omega$.

To obtain the stability condition of the second moment of the system (1), we multiply Eqs. (1) by $x_i, i = 1,2,\ldots,N$, respectively, and average them. Using $\mathrm{d}\langle x_i x_j\rangle/\mathrm{d}t = \langle \dot{x}_i x_j\rangle + \langle x_i \dot{x}_j\rangle$ to simplify these formulas, we have

$$
\begin{cases}
\left(\frac{\mathrm{d}}{\mathrm{d}t}+2\omega+2\varepsilon_1\right)\langle x_1^2\rangle-\varepsilon_1\langle x_1x_2\rangle-\varepsilon_1\langle x_2x_1\rangle+2\langle\xi x_1^2\rangle=A_0\cos(\Omega t)\langle x_i\rangle,\\
\left(\frac{\mathrm{d}}{\mathrm{d}t}+2\omega+2\varepsilon_1+\varepsilon_2\right)\langle x_1x_j\rangle-\varepsilon_2\langle x_1x_{j-1}\rangle-\varepsilon_1\langle x_1x_{j+1}\rangle-\varepsilon_1\langle x_2x_j\rangle+2\langle\xi x_1x_j\rangle=A_0\cos(\Omega t)(\langle x_1\rangle+\langle x_j\rangle),\quad 1<j<N,\\
\left(\frac{\mathrm{d}}{\mathrm{d}t}+2\omega+\varepsilon_1+\varepsilon_2\right)\langle x_1x_N\rangle-\varepsilon_1\langle x_2x_N\rangle-\varepsilon_2\langle x_1x_{N-1}\rangle+2\langle\xi x_1x_N\rangle=A_0\cos(\Omega t)(\langle x_1\rangle+\langle x_N\rangle)\\
\left(\frac{\mathrm{d}}{\mathrm{d}t}+2\omega+2\varepsilon_1+\varepsilon_2\right)\langle x_ix_1\rangle-\varepsilon_2\langle x_{i-1}x_1\rangle-\varepsilon_1\langle x_{i+1}x_1\rangle-\varepsilon_1\langle x_ix_2\rangle+2\langle\xi x_ix_1\rangle=A_0\cos(\Omega t)(\langle x_i\rangle+\langle x_1\rangle),\quad 1<i<N,\\
\left(\frac{\mathrm{d}}{\mathrm{d}t}+2\omega+2\varepsilon_1+2\varepsilon_2\right)\langle x_ix_j\rangle-\varepsilon_2\langle x_{i-1}x_j\rangle-\varepsilon_2\langle x_ix_{j-1}\rangle-\varepsilon_1\langle x_{i+1}x_j\rangle-\varepsilon_1\langle x_ix_{j+1}\rangle\\
+2\langle\xi x_ix_j\rangle=A_0\cos(\Omega t)(\langle x_i\rangle+\langle x_j\rangle),\quad 1<i,j<N,\\
\left(\frac{\mathrm{d}}{\mathrm{d}t}+2\omega+\varepsilon_1+2\varepsilon_2\right)\langle x_ix_N\rangle-\varepsilon_1\langle x_{i+1}x_N\rangle-\varepsilon_2\langle x_{i-1}x_N\rangle-\varepsilon_2\langle x_ix_{N-1}\rangle+2\langle\xi x_ix_N\rangle=A_0\cos(\Omega t)(\langle x_i\rangle+\langle x_N\rangle),\quad 1<i<N,\\
\left(\frac{\mathrm{d}}{\mathrm{d}t}+2\omega+\varepsilon_1+\varepsilon_2\right)\langle x_Nx_1\rangle-\varepsilon_1\langle x_Nx_2\rangle-\varepsilon_2\langle x_{N-1}x_1\rangle+2\langle\xi x_Nx_1\rangle=A_0\cos(\Omega t)(\langle x_N\rangle+\langle x_1\rangle)\\
\left(\frac{\mathrm{d}}{\mathrm{d}t}+2\omega+\varepsilon_1+2\varepsilon_2\right)\langle x_Nx_j\rangle-\varepsilon_1\langle x_Nx_{j+1}\rangle-\varepsilon_2\langle x_Nx_{j-1}\rangle-\varepsilon_2\langle x_{N-1}x_j\rangle+2\langle\xi x_Nx_j\rangle=A_0\cos(\Omega t)(\langle x_N\rangle+\langle x_j\rangle),\quad 1<i<N,\\
\left(\frac{\mathrm{d}}{\mathrm{d}t}+2\omega+2\varepsilon_2\right)\langle x_N^2\rangle-\varepsilon_2\langle x_{N-1}x_N\rangle-\varepsilon_2\langle x_Nx_{N-1}\rangle+2\langle\xi x_N^2\rangle=A_0\cos(\Omega t)(2\langle x_N\rangle).
\end{cases}
\tag{A5}
$$

To solve the new coupling term $\langle\xi x_ix_j\rangle$, we multiply Eqs. (1) by ξx_i, respectively, and average them. By Shapiro–Loginov formula, we obtain

$$
\begin{cases}
\left(\frac{\mathrm{d}}{\mathrm{d}t}+2\omega+2\varepsilon_1+\lambda\right)\langle\xi x_1^2\rangle-2\varepsilon_1\langle\xi x_1x_2\rangle+2\sigma^2\langle x_1^2\rangle=2A_0\cos(\Omega t)\langle\xi x_i\rangle,\\
\left(\frac{\mathrm{d}}{\mathrm{d}t}+2\omega+2\varepsilon_1+\varepsilon_2+\lambda\right)\langle\xi x_1x_j\rangle-\varepsilon_2\langle\xi x_1x_{j-1}\rangle-\varepsilon_1\langle\xi x_1x_{j+1}\rangle-\varepsilon_1\langle\xi x_2x_j\rangle+2\sigma^2\langle x_1x_j\rangle\\
=A_0\cos(\Omega t)(\langle\xi x_1\rangle+\langle\xi x_j\rangle),\quad 1<j<N,\\
\left(\frac{\mathrm{d}}{\mathrm{d}t}+2\omega+\varepsilon_1+\varepsilon_2+\lambda\right)\langle\xi x_1x_N\rangle-\varepsilon_1\langle\xi x_2x_N\rangle-\varepsilon_2\langle\xi x_1x_{N-1}\rangle+2\sigma^2\langle x_1x_N\rangle=A_0\cos(\Omega t)(\langle\xi x_1\rangle+\langle\xi x_N\rangle),\\
\left(\frac{\mathrm{d}}{\mathrm{d}t}+2\omega+2\varepsilon_1+\varepsilon_2+\lambda\right)\langle\xi x_ix_1\rangle-\varepsilon_2\langle\xi x_{i-1}x_1\rangle-\varepsilon_1\langle\xi x_{i+1}x_1\rangle-\varepsilon_1\langle\xi x_ix_2\rangle+2\sigma^2\langle x_ix_1\rangle\\
=A_0\cos(\Omega t)(\langle\xi x_i\rangle+\langle\xi x_1\rangle),\quad 1<i<N,\\
\left(\frac{\mathrm{d}}{\mathrm{d}t}+2\omega+2\varepsilon_1+2\varepsilon_2+\lambda\right)\langle\xi x_ix_j\rangle-\varepsilon_2\langle\xi x_{i-1}x_j\rangle-\varepsilon_2\langle\xi x_ix_{j-1}\rangle-\varepsilon_1\langle\xi x_{i+1}x_j\rangle-\varepsilon_1\langle\xi x_ix_{j+1}\rangle\\
+2\sigma^2\langle x_ix_j\rangle=A_0\cos(\Omega t)(\langle\xi x_i\rangle+\langle\xi x_j\rangle),\quad 1<i,j<N,\\
\left(\frac{\mathrm{d}}{\mathrm{d}t}+2\omega+\varepsilon_1+2\varepsilon_2+\lambda\right)\langle\xi x_ix_N\rangle-\varepsilon_1\langle\xi x_{i+1}x_N\rangle-\varepsilon_2\langle\xi x_{i-1}x_N\rangle-\varepsilon_2\langle\xi x_ix_{N-1}\rangle+2\sigma^2\langle x_ix_N\rangle\\
=A_0\cos(\Omega t)(\langle\xi x_i\rangle+\langle\xi x_N\rangle),\quad 1<i<N,\\
\left(\frac{\mathrm{d}}{\mathrm{d}t}+2\omega+\varepsilon_1+\varepsilon_2+\lambda\right)\langle\xi x_Nx_1\rangle-\varepsilon_1\langle\xi x_Nx_2\rangle-\varepsilon_2\langle\xi x_{N-1}x_1\rangle+2\sigma^2\langle x_Nx_1\rangle=A_0\cos(\Omega t)(\langle\xi x_N\rangle+\langle\xi x_1\rangle),\\
\left(\frac{\mathrm{d}}{\mathrm{d}t}+2\omega+\varepsilon_1+2\varepsilon_2+\lambda\right)\langle\xi x_Nx_i\rangle-\varepsilon_1\langle\xi x_Nx_{i+1}\rangle-\varepsilon_2\langle\xi x_Nx_{i-1}\rangle-\varepsilon_2\langle\xi x_{N-1}x_i\rangle+2\sigma^2\langle x_Nx_i\rangle\\
=A_0\cos(\Omega t)(\langle\xi x_N\rangle+\langle\xi x_i\rangle),\quad 1<i<N,\\
\left(\frac{\mathrm{d}}{\mathrm{d}t}+2\omega+2\varepsilon_2+\lambda\right)\langle x_N^2\rangle-2\varepsilon_2\langle\xi x_{N-1}x_N\rangle+2\sigma^2\langle x_N^2\rangle=A_0\cos(\Omega t)(2\langle\xi x_N\rangle).
\end{cases}
\tag{A6}
$$

Equations (A5) and (A6) can be written in the following matrix form:

$$
\frac{\mathrm{d}}{\mathrm{d}t}\boldsymbol{Y}+\hat{\boldsymbol{U}}\boldsymbol{Y}=\boldsymbol{F},
\tag{A7}
$$

where, $\boldsymbol{Y}=(\langle x_1^2\rangle,\ldots,\langle x_ix_j\rangle,\ldots,\langle x_N^2\rangle,\langle\xi x_1^2\rangle,\ldots,\langle\xi x_ix_j\rangle,\ldots,\langle\xi x_N^2\rangle)$, it contains $2N^2$ components.

$$
\boldsymbol{F}=A_0\cos(\Omega t)(\langle 2x_1\rangle,\ldots,\langle x_i\rangle+\langle x_j\rangle,\ldots,\langle 2x_N\rangle,\langle 2\xi x_1\rangle,\ldots,\langle\xi x_i\rangle+\langle\xi x_j\rangle,\ldots,\langle 2\xi x_N\rangle),
$$

$$
\hat{\boldsymbol{U}}=\begin{pmatrix}\Gamma & 2E\\ 2\sigma^2E & \lambda E+\Gamma\end{pmatrix},
$$

$$
\Gamma=\begin{pmatrix}
U_1 & -\varepsilon_1E & & & \\
-\varepsilon_2E & U_2 & -\varepsilon_1E & & \\
 & & \ddots & & \\
 & & -\varepsilon_2E & U_2 & -\varepsilon_1E\\
 & & & -\varepsilon_2E & U_3
\end{pmatrix},
$$

where, $U_1 = U + (\omega+\varepsilon_1)E$, $U_2 = U + (\omega+\varepsilon_1+\varepsilon_2)E$, $U_3 = U + (\omega+\varepsilon_2)E$.

The characteristic equation of Eq. (A7) is $|sE+\hat{U}|$. The stability of the second moment of the system (1) is equivalent to the fact that all roots of the characteristic equation $|sE+\hat{U}|$ are distributed in the right-half complex plane, that is, the eigenvalues of matrix $\hat{U}$ are all distributed in the right-half complex plane.

Theorem A2 The second moment of particles displacements of the asymmetric nearest neighbor coupled system (1) is stable if and only if $\sigma^2 < \sigma^2_{\rm sta2} = \omega^2 + \frac{1}{2}\lambda\omega$.

Proof Because matrix $\hat{U}$ has the same form as matrix $\tilde{U}$ in Eq. (A2). It can be derived by analogy that the eigenvalues of $\hat{U}$ are distributed in the right half complex plane if and only if $\sigma^2 < \frac{1}{4}(r^2_{\rm sta2} + \lambda r_{\rm sta2})$. Where $r_{\rm sta2}$ is the minimum eigenvalue of the matrix Γ. The sum of each row in Γ is 2ω, that is, 2ω is a factor of the determinant of Γ. Thus, 2ω is an eigenvalue of Γ. From Gerschgorin circle theorem, 2ω is the smallest eigenvalue. Thus, $r_{\rm sta2} = 2\omega$, and $\frac{1}{4}(r^2_{\rm sta2} + \lambda r_{\rm sta2}) = \omega^2 + \frac{1}{2}\lambda\omega$. The stability condition of the second moment of the system (1) becomes $\sigma^2 < \omega^2 + \frac{1}{2}\lambda\omega$.

Appendix B: Appendix for Subsection 3.1.2

To solve the synchronization condition of the system (1), take the average of both sides of Eq. (8), we have

$$\begin{cases} \left(\dfrac{\mathrm{d}}{\mathrm{d}t} + \omega + \varepsilon_1 + \varepsilon_2\right)\langle\delta_1\rangle + \langle\xi\,\delta_1\rangle - \varepsilon_1\langle\delta_2\rangle = 0, \\ \left(\dfrac{\mathrm{d}}{\mathrm{d}t} + \omega + \varepsilon_1 + \varepsilon_2\right)\langle\delta_i\rangle + \langle\xi\,\delta_i\rangle - \varepsilon_1\langle\delta_{i+1}\rangle \\ -\varepsilon_2\langle\delta_{i-1}\rangle = 0, \quad 1 < i < N-1, \\ \left(\dfrac{\mathrm{d}}{\mathrm{d}t} + \omega + \varepsilon_1 + \varepsilon_2\right)\langle\delta_{N-1}\rangle + \langle\xi\,\delta_{N-1}\rangle - \varepsilon_2\langle\delta_{N-2}\rangle = 0. \end{cases} \tag{B1}$$

A new variable $\langle\xi\,\delta_i\rangle$ appeared in Eq. (4). Multiplying (4) by ξ and then averaging, we get the following $N-1$ linear differential equations

$$\begin{cases} \left(\dfrac{\mathrm{d}}{\mathrm{d}t} + \lambda + \omega + \varepsilon_1 + \varepsilon_2\right)\langle\xi\,\delta_1\rangle + \sigma^2\langle\delta_1\rangle - \varepsilon_1\langle\xi\,\delta_2\rangle = 0, \\ \left(\dfrac{\mathrm{d}}{\mathrm{d}t} + \lambda + \omega + \varepsilon_1 + \varepsilon_2\right)\langle\xi\,\delta_i\rangle + \sigma^2\langle\delta_i\rangle \\ -\varepsilon_1\langle\xi\,\delta_{i+1}\rangle - \varepsilon_2\langle\xi\,\delta_{i-1}\rangle = 0, \quad 1 < i < N-1, \\ \left(\dfrac{\mathrm{d}}{\mathrm{d}t} + \lambda + \omega + \varepsilon_1 + \varepsilon_2\right)\langle\xi\,\delta_{N-1}\rangle \\ +\sigma^2\langle\delta_{N-1}\rangle - \varepsilon_2\langle\xi\,\delta_{N-2}\rangle = 0. \end{cases} \tag{B2}$$

Equations (B1) and (B2) can be written in the following matrix form:

$$\frac{\mathrm{d}\tilde{\delta}}{\mathrm{d}t} + \tilde{V}\tilde{\delta} = 0, \tag{B3}$$

where, $\tilde{\delta} = (\langle\widetilde{\delta}_1\rangle, \ldots, \langle\widetilde{\delta}_{N-1}\rangle, \langle\xi\,\widetilde{\delta}_1\rangle, \ldots, \langle\xi\,\widetilde{\delta}_{N-1}\rangle)$,

$$\tilde{V} = \begin{pmatrix} V & E \\ \sigma^2 E & \lambda E + V \end{pmatrix},$$

where

$$V = \begin{pmatrix} \omega+\varepsilon_1+\varepsilon_2 & -\varepsilon_1 & & & \\ -\varepsilon_2 & \omega+\varepsilon_1+\varepsilon_2 & -\varepsilon_1 & & \\ & & \ddots & & \\ & & -\varepsilon_2 & \omega+\varepsilon_1+\varepsilon_2 & -\varepsilon_1 \\ & & & -\varepsilon_2 & \omega+\varepsilon_1+\varepsilon_2 \end{pmatrix},$$

$\tilde{\delta} = 0$ is obviously a solution of Eq. (B3) under zero initial value conditions. This means that the system (1) is synchronous. When the equation system (B3) is stable, the initial value does not affect the motion state of the particles after a period of time. So when equation (B3) is stable, the system (1) is statistics synchronization.

Theorem B1 The system (1) is statistics synchronization if and only if $\sigma^2 < \sigma^2_{\rm syn} = r^2_{\rm syn} + \lambda r_{\rm syn}$, where

$$r_{\rm syn} = \omega + \varepsilon_1 + \varepsilon_2 + 2\sqrt{\varepsilon_1\varepsilon_2}\cos\frac{(N-1)\pi}{N}.$$

Proof The statistical synchronization of the system (1) is equivalent to the fact that all eigenvalues of the matrix $\tilde{V}$ are distributed in the right-half complex plane. And $\tilde{V}$ has the same form as matrix $\tilde{U}$ in Eq. (A2). It can be deduced by analogy that the eigenvalues of matrix $\tilde{V}$ are distributed in the right-half complex plane if and only if $\sigma^2 < r^2_{\rm syn} + \lambda r_{\rm syn}$. $r_{\rm syn}$ is the minimum eigenvalue of the matrix V. According to Ref. [55], we obtain

$$r_{\rm syn} = \omega + \varepsilon_1 + \varepsilon_2 + 2\sqrt{\varepsilon_1\varepsilon_2}\cos\frac{(N-1)\pi}{N}.$$

Acknowledgement

Project supported by the Natural Science Foundation of Shandong Province of China for the Youth (Grant No. ZR2023QA102).

References

[1] Barzel B and Barabási A L 2013 *Nat. Phys.* **9** 673
[2] Zheng Z 2019 *Emergence dynamics in complex systems: from synchronization to collective transport-i* (Beijing: Science Press) (in Chinese)
[3] Boccaletti S, Latora V, Moreno Y, Chavez M and Hwang D U 2006 *Phys. Rep.* **424** 175
[4] Acebrón J A, Bonilla L L, Vicente C J P, Ritort F and Spigler R 2005 *Rev. Mod. Phys.* **77** 137
[5] Boccaletti S, Bianconi G, Criado R, Del Genio C I, Gómez-Gardenes J, Romance M, Sendina-Nadal I, Wang Z and Zanin M 2014 *Phys. Rep.* **544** 1
[6] Ghosh S, Rangarajan G and Sinha S 2010 *Europhys. Lett.* **92** 40012
[7] Dorfler F and Bullo F 2012 *SIAM J. Control Optim.* **50** 1616
[8] Yang B, Zhang X, Zhang L and Luo M K 2016 *Phys. Rev. E* **94** 022119
[9] Zhang L, Xu L, Yu T, Lai L and Zhong S C 2021 *Commun. Nonlinear Sci.* **93** 105499
[10] Xu C, Sun Y T, Gao J, Jia WJ and Zheng Z G 2018 *Nonlinear Dynam.* **94** 1267
[11] Perc M 2007 *Phys. Rev. E* **76** 066203

[12] Pikovsky A, Rosenblum V and Kurths J 2001 *Synchronization: A Universal Concept in Nonlinear Sciences* (New York: Cambridge University Press)
[13] Yang P, Liu F, Liu T and Hill D J 2023 *IEEE Trans. Autom. Control.* 1
[14] Sarfati R, Hayes J C and Peleg O 2021 *Sci. Adv.* **7** eabg9259
[15] Lai Y M and Porter M A 2013 *Phys. Rev. E* **88** 012905
[16] Khalil H K 2002 *Automatica* **38** 1091
[17] Gammaitoni L, Hänggi P, Jung P and Marchesoni F 1998 *Rev. Mod. Phys.* **70** 223
[18] Rozenfeld R, Freund J A, Neiman A and Schimansky-Geier L 2001 *Phys. Rev. E* **64** 051107
[19] Zhou C and Kurths J 2002 *Phys. Rev. Lett.* **88** 230602
[20] Häunggi P and Jung P 1994 *Adv. Chem. Phys.* **89** 239
[21] Sastry S 2013 *Nonlinear systems: analysis, stability, and control*, Vol. 10 (Springer Science & Business Media)
[22] Wang Z and Liu Z 2020 *Acta Phys. Sin.* **69** 088902 (in Chinese)
[23] Zhang Y, Hu G and Gammaitoni L 1998 *Phys. Rev. E* **58** 2952
[24] Powanwe A S and Longtin A 2020 *Phys. Rev. Res.* **2** 043067
[25] Cantos C E, Hammond D K and Veerman J 2016 *Eur. Phys. J. Special Topics* **225** 1199
[26] Gupta A K 2016 *J. Stat. Phys.* **162** 1571
[27] Hillier D, Günel S, Suykens J A and Vandewalle J 2007 *Int. J. Bifurcat. Chaos* **17** 4177
[28] Palacios A 2021 *Phys. Rev. E* **103** 022206
[29] Batra P and Chopra R 2021 *Physica A* **561** 125148
[30] Elvira K S, Solvas X C, Wootton R C and Demello A J 2013 *Nat. Chem.* **5** 905
[31] Ai B Q and Liu L G 2006 *Phys. Rev. E* **74** 051114
[32] Burada P S, Schmid G, Reguera D, Vainstein MH, Rubi J and Hänggi P 2008 *Phys. Rev. Lett.* **101** 130602
[33] Zhang L, Lai L, Peng H, Tu Z and Zhong S 2018 *Phys. Rev. E* **97** 012147
[34] Chen X, Luo M, Zhong Y and Zhang L 2022 *Physica A* **605** 128006
[35] Li J h, Chen Q h and Zhou X f 2010 *Phys. Rev. E* **81** 041104
[36] Lv J P, Liu H and Chen Q H 2009 *Phys. Rev. B* **79** 104512
[37] Wang Q, Perc M, Duan Z and Chen G 2009 *Chaos* **19** 023112
[38] Van Den Broeck C 1983 *J. Stat. Phys.* **31** 467
[39] Gammaitoni L, Maichesoni F, Menichella-Saetta and Santucci S 1989 *Phys. Rev. Lett.* **62** 349
[40] Bena I, Van den Broeck C, Kawai R and Lindenberg K 2002 *Phys. Rev. E* **66** 045603
[41] Li J h 2011 *Chaos* **21** 043115
[42] Berdichevsky V and Gitterman M 1996 *Europhys. Lett.* **36** 161
[43] Fuliński A 1993 *Phys. Lett. A* **180** 94
[44] Robertson B and Astumian R D 1991 *J. Chem. Phys.* **94** 7414
[45] Kubo R 1963 *J. Math. Phys.* **4** 174
[46] Hasty J, Pradines J, Dolnik M and Collins J J 2000 *Proc. Natl. Acad. Sci. USA* **97** 2075
[47] Li J H and Han Y X 2006 *Phys. Rev. E* **74** 051115
[48] Dorf R C and Bishop R H 2011 *Modern control systems* (Pearson)
[49] Yu T, Zhang L, Ji Y and Lai L 2019 *Commun. Nonlinear Sci.* **72** 26
[50] Kim C, Lee E K and Talkner P 2006 *Phys. Rev. E* **73** 026101
[51] Xu B, Duan F, Bao R and Li J 2002 *Chaos, Solitons and Fractals* **13** 633
[52] Liang X, Liu C and Zhang X 2020 *Phys. Rev. E* **101** 022205
[53] Liang X, Hua L, Zhang X and Zhao L 2022 *Phys. Rev. E* **106** 064306
[54] Varga R S 2010 *Geršgorin and his circles*, Vol. 36 (Springer Science & Business Media)
[55] Kulkarni D, Schmidt D and Tsui S K 1999 *Linear Algebra Appl.* **297** 63